Friedrich-Alexander-Universität
Faculty of Engineering

Practical: Atomistic Simulations

Leon Pyka (22030137), Alex Rausch(22268314)

Supervision: Zhipeng Yao

Contents

1 Introduction

In materials science and computational chemistry, atomistic simulation is one of the go-to methods for modeling systems. This method is decisively influenced by intricate effects occurring on an atomic scale, such as the presence of single-atom impurities, dislocations, and stacking faults. It becomes particularly relevant when meso-scale methods fall short in delivering the required accuracy. In scenarios where the precision of ab-initio methods, exemplified by *density functional theory* (DFT), is deemed unnecessary, the atomistic approach steps in as a pragmatic solution. By focusing on phenomena at the atomic level, this method strikes a balance between computational efficiency and capturing essential intricacies that elude coarser modeling techniques. In the course of this practical different atomistic simulations are carried out in the python ASE environment.

2 Task 2.1: Literature Research

The basis of atomistic simulation can be expressed as solving Newtons second equation for the atoms in the simulation box. See eq. 1a where m_i is every atoms mass $\ddot{x}_i$ the acceleration of every atom (as second time derivative of position) is calculated from potential U. U as presented in eq. 1b can be one-, two- or more body potential (depending on application). Typical potentials to be used in atomistic simulations are pair-potentials (e.g. the Lennard-Jones-Potential) or semi-empirical *Embedded Atom Method* (EAM) potentials such as *Effective-medium theory* (EMT).

$$m_i \ddot{x}_i = -\nabla_{x_i} U(x_1, x_2, ...x_N) \tag{1a}$$

$$U(x_1, x_2, ...x_N) = \sum_i V_1(x_i) + \sum_{i,j} V_2(x_i, x_j) + \sum_{i,j,k} V_3(x_i, x_j, x_k) + ... \tag{1b}$$

The *Lennard Jones* potential - see eq. 2 - is calculated with respect to r - the distance of the interacting particles, ϵ - the "depth" of the potential minimum and σ - the distance between the interacting particles at which the potential is 0. The exponents 12 and 6 are chosen for reasons of being easier to compute (12 being $6 * 2$). The variable a_i is the number of equidistant atoms associated with the nearest neighbour of atom i. Another point to notice is that the N-M potential is a generalized form of the LJ potential, with the exponents being variables - thus allowing for two more degrees of freedom for fitting. [7]

$$U_{LJ} = \Sigma_i \frac{a_i}{2} 4\epsilon \left[\left(\frac{\sigma}{r_i} \right)^{12} - \left(\frac{\sigma}{r_i} \right)^{6} \right] \tag{2}$$

$$U_{LJ,i} = 4\epsilon \left[\left(\frac{\sigma}{r} \right)^{12} - \left(\frac{\sigma}{r} \right)^{6} \right] \tag{3}$$

Pair-potentials such as the LJ potential is not suitable for the simulation of metals - often being referred to as "toy-potentials". They are lacking a term that is taking into account the delocalized, which is crucial for realistically modelling the mechanical properties of metals. Pair-potentials are much more suitable for e.g. describing van der Waals interactions

of molecules. An example where pair-potentials might be feasible is studying bonding behaviour that a semi-empirical potential might not have been fitted for, e.g. interaction between a substrate and foreign atoms during physical vapour deposition [7, 3]. EMT on the other hand first calculates the atoms energies in an effective medium. This ensures that when calculating the respective energy not only the distance of a second atom is taken into account but also taking into account the number and kind of other surrounding atoms. This is useful when e.g. simulating metals, assuming a uniform electron gas. Starting with the cohesive energy $E_{c,i}$ of an atom i, that is dependent on the embedding density n_i and then adding a correctional term [6]. The correctional term - being the difference between the energy of a real reference system and the sum of all cohesive energy terms ($E - \sum E_{c,i}$) - can be derived from DFT calculations. [6, 5]. The total energy of a system can be given as:

$$E = \sum_i E_{c,i} + \Delta E_{AS} + \Delta E_{1el} \tag{4}$$

where the added energy terms are the atomic-sphere correction term ΔE_{AS} and the one-electron correction ΔE_{1el}. For small ΔE_{1el}, a pair-potential approximation for ΔE_{AS} can be applied:

$$E = \sum_i \Big[E_{c,i}(n_i + \Delta E_{AS}(i) \Big] \tag{5a}$$

$$= \sum_i \Big\{ E_{c,i}(n_i) + \frac{1}{2} \Big[\sum_{i \neq j} V_{ij}(r_{ij}) - \sum_{i \neq j}^{ref} V_{ij}(r_{ij}) \Big] \Big\} \tag{5b}$$

The fitting paramters of EMT are E_0, s_0 - equilibrium neutral sphere radius, V_0 - which is derived from the shear modulus, η_2 - fall-off of electron density, κ, λ - derived from the bulk modulus, n_0 - the density parameter. In ASE there are implementations of EMT potentials. Tab. 1 shows fitting parameters for a copper lattice. Although an argument can be made that there are no "correct" fitting parameters for the LJ since it is not suitable to represent metals [14] efforts are still being made to create the best possible fit. An important note - results gained through any type of potential are only able to depict physical phenomena, that these potentials were designed/ fitted to match correctly.

Potential	Fitting parameters						
EMT	$E_0(eV)$	$s_0(bohr)$	$V_0(eV)$	$\eta_2(bohr^{-1})$	$\kappa(bohr^{-1})$	$\lambda(bohr^{-1})$	$n_0(bohr^{-3})$
	-3.51	2.67	2.476	1.652	2.740	1.906	0.00910
LJ	$\epsilon(eV)$	$\sigma(bohr)$					
	0.4099	4.411					

Table 1: Fitting parameters for Cu with EMT potential [5] and LJ potential[7].

3 Application of a atomistic code for determination of elastic constants and verification of potentials

The following section will be dedicated to assert, whether the chosen potential is fitting the systems we are looking to simulate. For this we compute the minimal energies for different crystal structures and elastic constants to compare them with literature values.

3.1 Task 3.1: Estimate lattice constant

As a starting point for our Molecular Static simulation we need to estimate the lattice constant L. Assuming the atoms to be spheres of radius $a = 128\ pm$ we can calculate L. Knowing that densest directions of the different crystal structures (SC - [1 0 0], BCC -[1 1 1], FCC - [1 1 0]) we can calculate the lattice constants utilizing the Pythagorean theorem as sketched in fig.1.

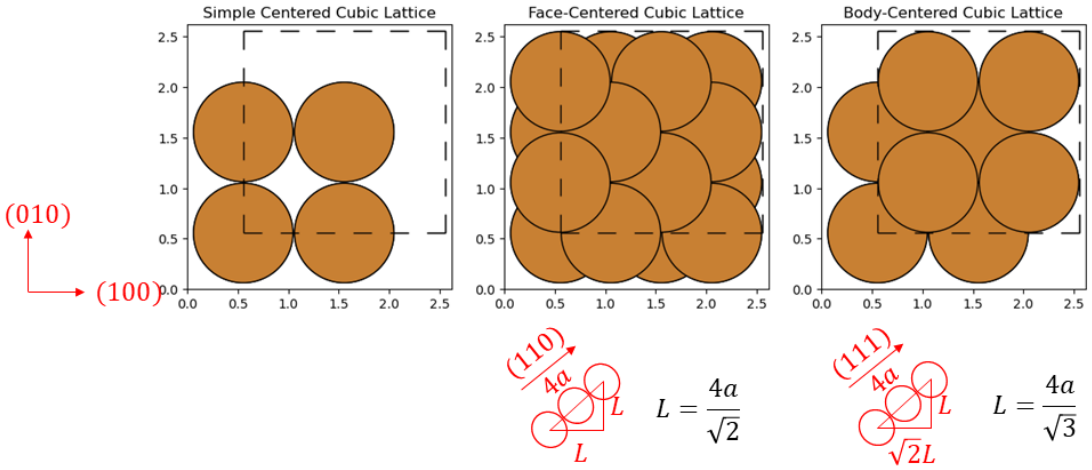

Figure 1: Sketch of simple, face-centered and body-centered crystal, with outline for calculating the corresponding lattice constants.

So the lattice constants are:

$$L_{SC} = 2a = 256\ pm \tag{6a}$$

$$L_{BCC} = \frac{4a}{\sqrt{3}} = 296\ pm \tag{6b}$$

$$L_{FCC} = \frac{4a}{\sqrt{2}} = 362\ pm \tag{6c}$$

3.2 Task 3.2: Calculate Lattice Constants via Molecular Statics

Here we generated SC, BCC and FCC crystals. Using the ASE library we create trajectories varying the lattice constants. As a starting point we the used the estimated values L_{est} from the previous section 3.1. We calculate the corresponding potential energies using the ASE native EMT potential for 100 steps from $L_{est} - 50\ pm$ to $L_{est} + 100\ pm$. We used a second order polynomial $W(L) = p_0 + p_1 L + p_2 L^2$ to fit the data. Setting the first derivative $dW(L) = p_1 + 2p_2$ to zero and solving for 0 gives us the minimal potential energy. The data can be fitted using the `scipy` package - the `scipy.opimize.curve_fit` function naturally uses the Levenberg-Marquardt algorithm [11]. The results are plotted in fig. 2. The FCC value differs from 361.46 pm as provided in the literature [4].

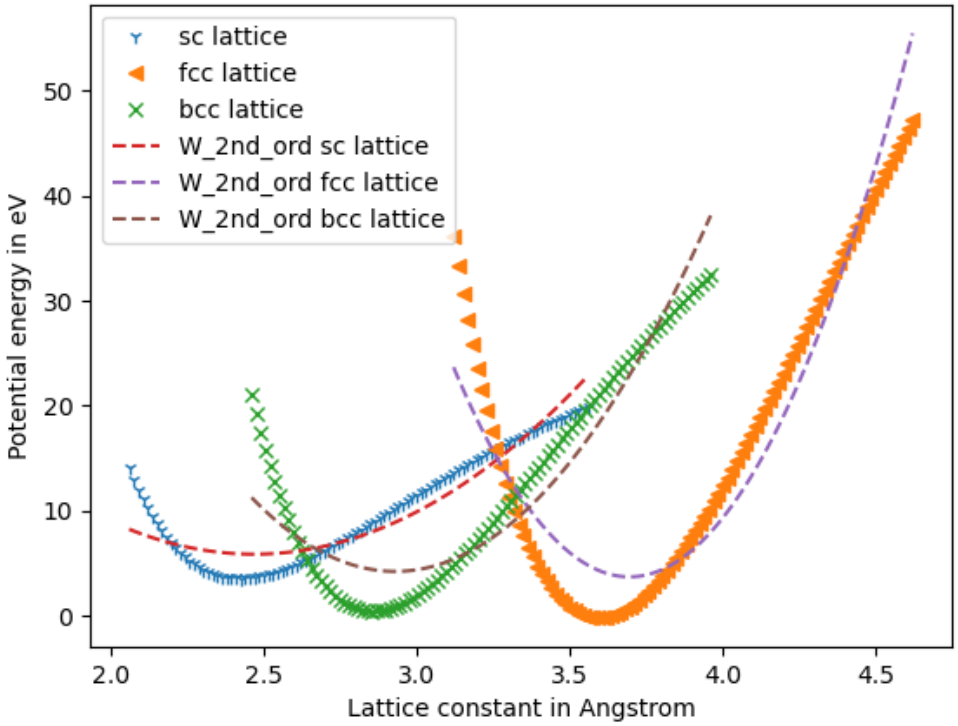

Figure 2: Potential Energies of the sc, bcc and fcc crystal for varying lattice constants. Fitting curves of second order polynomials are included.

Reducing the interval increases the accuracy of the fit. The results can be seen in fig. 3. Tab. 2 shows the calculated lattice constants. Even higher accuracy could be achieved using a third order polynomial.

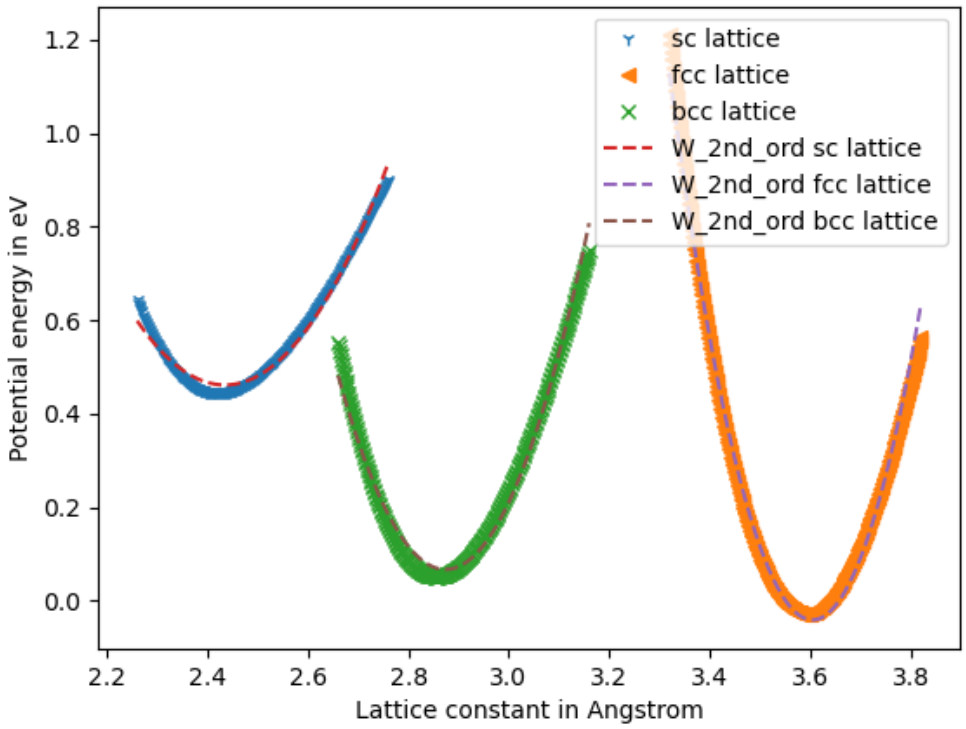

Figure 3: Potential Energies of the sc, bcc and fcc crystal for varying lattice constants. Fitting curves of second order polynomials are included.

3.3 Task 3.3: Derivation of elastic constants of isotropic media

To calculate C_{12} from the strain energy density W^e - assuming we know C_{11} from $C_{11} = \frac{2W^e}{\epsilon_1 \cdot \epsilon_1}$.

$$W^e = \frac{1}{2} \begin{bmatrix} \epsilon_1 \\ \epsilon_2 \\ 0 \\ 0 \\ 0 \\ 0 \end{bmatrix}^T \begin{bmatrix} C_{11} & C_{12} & C_{12} & 0 & 0 & 0 \\ C_{12} & C_{11} & C_{12} & 0 & 0 & 0 \\ C_{12} & C_{12} & C_{11} & 0 & 0 & 0 \\ 0 & 0 & 0 & \frac{C_{11}-C_{12}}{2} & 0 & 0 \\ 0 & 0 & 0 & 0 & \frac{C_{11}-C_{12}}{2} & 0 \\ 0 & 0 & 0 & 0 & 0 & \frac{C_{11}-C_{12}}{2} \end{bmatrix} \begin{bmatrix} \epsilon_1 \\ \epsilon_2 \\ 0 \\ 0 \\ 0 \\ 0 \end{bmatrix} \tag{7a}$$

$$= \frac{1}{2}(C_{11}\epsilon_1^2 + 2C_{12}\epsilon_1\epsilon_2 + C_{11}\epsilon_2^2) \tag{7b}$$

$$C_{12} = \frac{2W^e - C_{11}(\epsilon_1^2 + \epsilon_2^2)}{2\epsilon_1\epsilon_2} \tag{7c}$$

Second order polynomial fit	
SC	243.48 pm
BCC	287.40 pm
FCC	360.45 pm

Table 2: Lattice constant derived from polynomial fits to the potential energy.

3.4 Task 3.4: Calculating the Elastic Constants for Cubic Symmetry

For cubic symmetry C_{44} needs to be calculated separately - while in isotropic materials it is equal to $\frac{C_{11}-C_{12}}{2}$.

$$W^e = \frac{1}{2}\begin{bmatrix} 0 \\ 0 \\ 0 \\ 2\epsilon_{12} \\ 0 \\ 0 \end{bmatrix}^T \begin{bmatrix} C_{11} & C_{12} & C_{12} & 0 & 0 & 0 \\ C_{12} & C_{11} & C_{12} & 0 & 0 & 0 \\ C_{12} & C_{12} & C_{11} & 0 & 0 & 0 \\ 0 & 0 & 0 & C_{44} & 0 & 0 \\ 0 & 0 & 0 & 0 & C_{44} & 0 \\ 0 & 0 & 0 & 0 & 0 & C_{44} \end{bmatrix} \begin{bmatrix} 0 \\ 0 \\ 0 \\ 2\epsilon_{12} \\ 0 \\ 0 \end{bmatrix} = \tag{8a}$$

$$= 2\epsilon_{12}\epsilon_{12}C_{44} \tag{8b}$$

$$C_{44} = \frac{W^e}{2\epsilon_{12}\epsilon_{12}} \tag{8c}$$

Notice that ϵ_{12} is interchangeable - meaning that C_{44} is the same for $\epsilon_{12} = \epsilon_{13} = \epsilon_{23}$.

3.5 Task 3.5: Molecular Statics for Computing the Elastic Constants

For computing the elastic constants we first create a copper FCC lattice utilizing the lattice constant from section 3.2. Before straining the specimen, it is relaxed via the atomistic structure optimization algorithm FIRE [1]. We then vary the cell-dimensions and the atoms positions in the cell via matrix multiplication for three different cases of deformation - uniaxial, biaxial and shear:

$$uniaxial: \begin{bmatrix} 1+\epsilon & 0 & 0 \\ 0 & 1 & 0 \\ 0 & 0 & 1 \end{bmatrix} \tag{9a}$$

$$biaxial: \begin{bmatrix} 1+\epsilon & 0 & 0 \\ 0 & 1+\epsilon & 0 \\ 0 & 0 & 1 \end{bmatrix} \tag{9b}$$

$$shear: \begin{bmatrix} 1 & \epsilon & 0 \\ \epsilon & 1 & 0 \\ 0 & 0 & 1 \end{bmatrix} \tag{9c}$$

$$\tag{9d}$$

To get a good range to fit over the ϵ values are varied accordingly. The resulting deformed cells are relaxed once again, before calculating the potential energy. Plotting the varying strain ϵ against the potential energies yields fig. 4. Fitting a third order polynomial $W_f^e = p_0 + p_1\epsilon + p_2\epsilon^2 + p_3\epsilon^3$ via `scipy.opimize.curve_fit` - as was done in section 3.2 - allows further investigation of the curve. The root of the first derivative of the fitting function $\frac{dW_f^e}{d\epsilon} = p_1 + 2p_2\epsilon_{min} + 3p_3\epsilon_{min}^2 = 0$ gives the associated ϵ_{min} at which the potential energy is minimal. The third derivative of the fitting function evaluated at ϵ_{min} is a value, representing an elastic constant (in the case of C_{11}) or a combination of these. In the strain tensors used ϵ so that $\epsilon_{11} = \epsilon 12$. So from eq. 7b we can derive the second derivative:

$$W^e = \frac{1}{2}(2\epsilon^2 C_{11} + 2\epsilon^2 C_{12}) \tag{10a}$$

$$\frac{d^2W^e}{d\epsilon^2} = 2C_{11} + 2C_{12} \tag{10b}$$

$$\rightarrow C_{12} = \frac{1}{2}(\frac{d^2W^e}{d\epsilon^2} - 2C_{11}) \tag{10c}$$

where $\frac{d^2W^e}{d\epsilon^2}$ is approximated at ϵ_{min} as $\frac{d^2W_f^e(\epsilon_{min})}{d\epsilon^2} = 2p_2 + 6p_3\epsilon_{min}$

For comparison the results are then multiplied with a factor of 1.6021 for unit conversion from eV/Angstrom to N/mm^2. The results are shown in tab. 3 - alongside experimental reference values.

	Constant	Modelling	Experimental Results	Error in %
	C_{11}	1.6469	1.7620	6.53
	C_{12}	1.2965	1.2494	3.77
c_44	C_{12}	0.8492	0.8177	3.86

Table 3: Results for elastic constants in $10^{11}\frac{N}{m^2}$ of Molecular Static Modeling compared to experimental results [12].

3.6 Task 3.6: Boundaries for assuming quadratic dependency of strain-energy density

Looking at the plot (fig. 5) of bigger strains we see, that strains higher than $\epsilon = 0.2$ the assumption of quadratic dependency of energy density to strain is no longer feasible. Plotting the corresponding derivatives of the fitting functions (fig. 6) allows the conclusion that - judging from the local minimum in the first and the related zero position in the second derivative - the function switches from concave up to concave down movement. This fact is supporting that in the latest at this point the trajectory of the energy density with respect to the strain is showing behaviour of functions of higher grade than two.

Straining for ϵ values higher than 0.2 results in deviations and the fitting failing, as is evident in fig. 7. For uniaxial strain it seems the fit seems to deviate a little bit later as

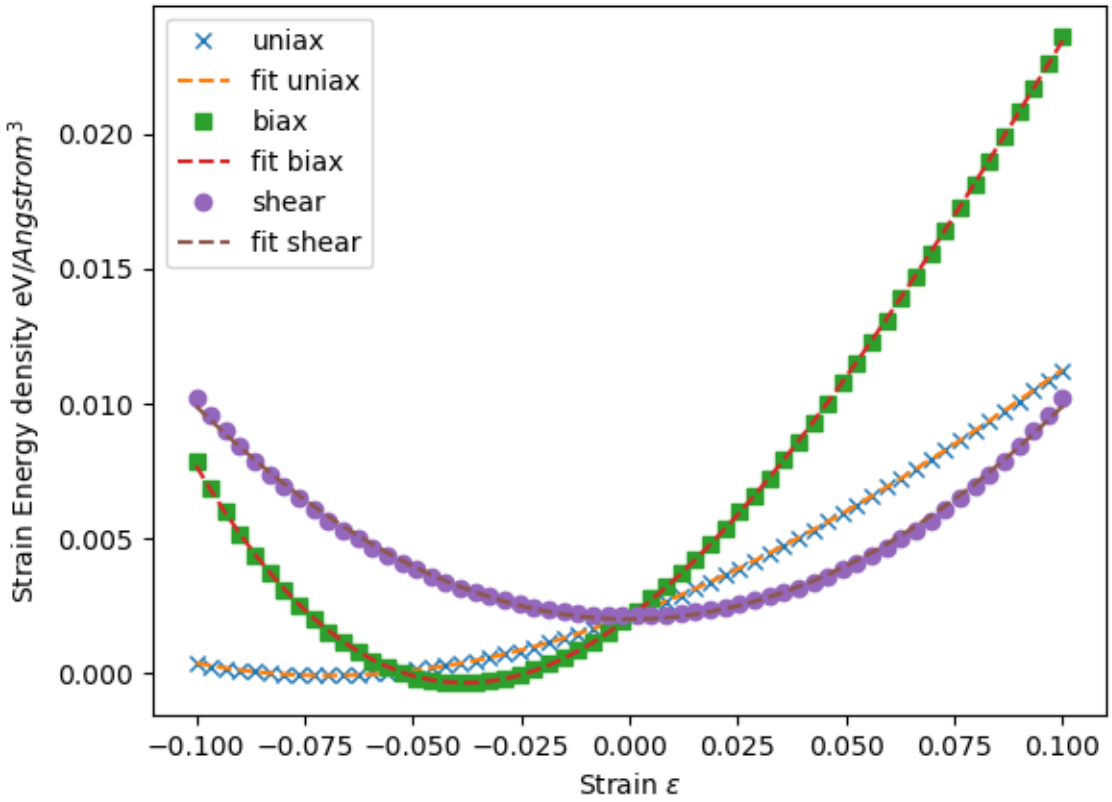

Figure 4: Plot of ϵ against potential energy density for uniaxial and biaxial strain and shear, with third order polynomial fit.

can be seen in fig. 8 .

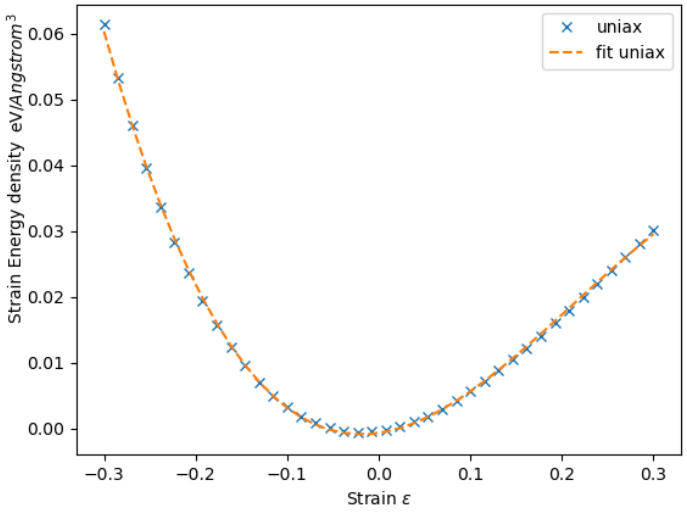

Figure 5: Plot of ϵ against strain energy density for strain.

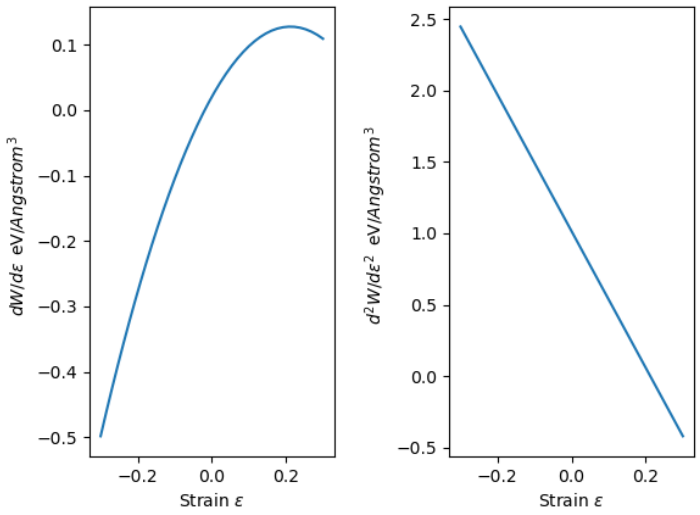

Figure 6: Plot of the derivatives of the fitting function.

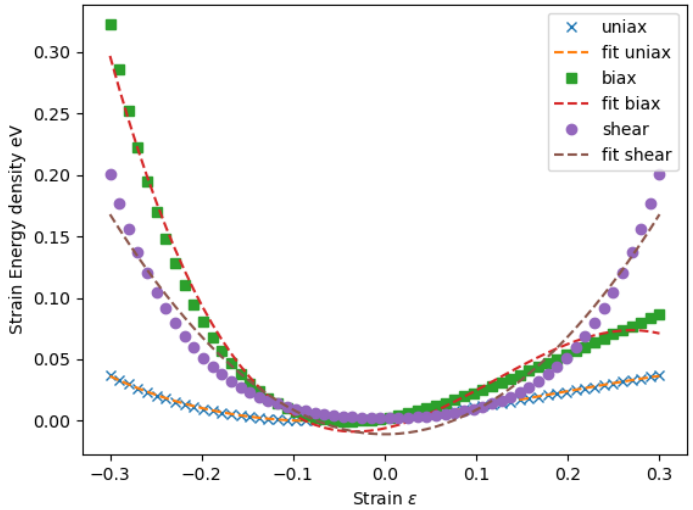

Figure 7: Plot of strain energy density at strains higher than $\epsilon = 0.2$.

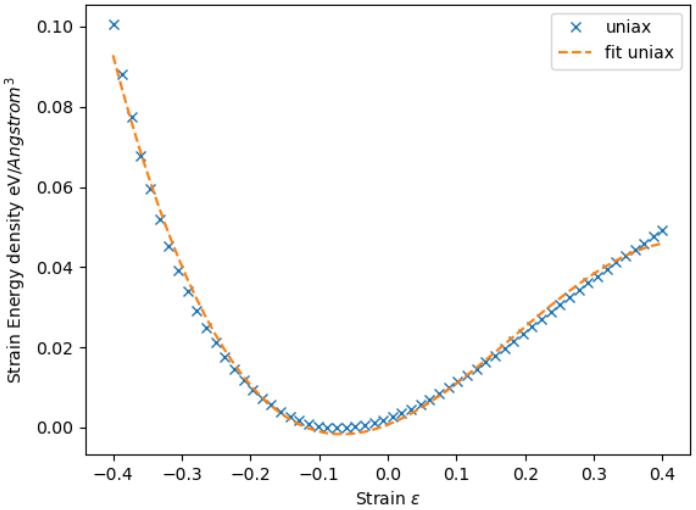

Figure 8: Plot of strain energy density at uniaxial strains higher than $\epsilon = 0.2$.

4 Molecular Dynamics simulation of bond breaking of carbon nano-tubes

The following tasks are dedicated to investigating *carbon nano-tubes* (CNT). Running molecular dynamic simulations to model the bond breaking behaviour of CNTs.

4.1 Task 4.1: Literature research - different CNTs

Carbon nano-tubes essentially consist graphene sheets. Graphene being a polyaromatic monoatomic layer of sp^2-hybridized carbon atoms - compared to graphite, which consists of multiple layers of graphene. The graphene is rolled into a cylinder, coherently connecting the aromatic rings. The tips are sealed by hemi-fullerenes [10]. The design of a CNT is also includes structures where CNTs are contained within another CNT. These are called *multi-wall carbon nano-tubes* (MWNT). If the CNT consists of just one layer of graphen, these are called *single-wall carbon nano-tubes* (SWNT). Fig. 9 shows three different types of CNT - namelely:

- zig-zag-type
- armchair-type
- helical

Simply by looking at the structure of a CNT it can be assumed, that it should withstand high stress in longitudinal direction and show brittle behaviour. The C atoms are each in a covalent bond with their neighbours. For the following simulations a (5,5) armchair nano-tube is chosen.

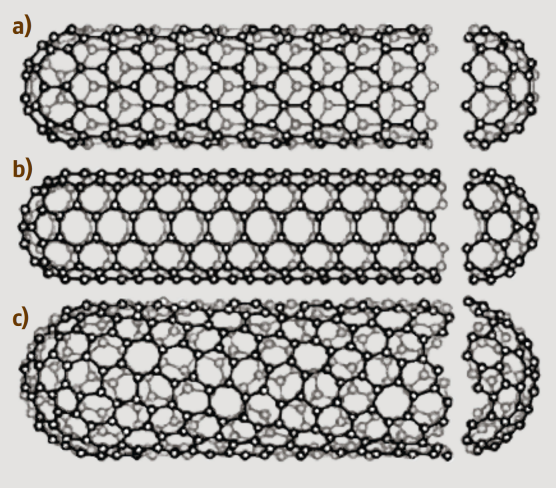

Figure 9: Sketches of three different SWNT structures that are examples of (a) a zig-zag-type nanotube, (b) an armchair-type nanotube, (c) a helical nanotube. Reproduced from [10].

4.2 Task 4.2: Setting up NVE-Simulations of Strain on CNTs

To have an initial starting point for strain rates and failure strain we refer to the respective sources. Critical strain can be found to be at approximately 20 - 40% [15] and strain rates that are referred to as high rates are found to be at $3000s^{-1}$[8]. The velocity-verlet algorithm calculates the positions and velocities of the atoms after a timestep Δt. The number of times the verlet algorithm is executed will be denoted as N_v. For the simulation the sample is deformed by $\epsilon_i \cdot L_{init}$ where ϵ_i is the increment of the applied strain and L_{init} is the initial length of the CNT. The CNT is generated with periodic boundary conditions along the z-axis - using the `ase.build.nanotube` method. The total strain is defined by the number of times N_i the incremental length is added to the cells length in z-direction and the atoms are scaled accordingly - see eq. 11a. The strain rate $\dot{\epsilon}$ is given by the time, the simulation rests at the new, deformed state - which is depending on N_v and Δt.

$$\epsilon_{tot} = N_i \epsilon_i \tag{11a}$$

$$\dot{\epsilon} = \frac{\epsilon_i}{N_v \Delta t} \tag{11b}$$

$$\tag{11c}$$

For the simulation the CNT is created via the `ase.build.nanotube` method, with a length of 3 and periodic boundary conditions in the longetudinal direction (the z-axis) - resulting in a nanotube of 3 repeating units within the simulation cell. The particles momenta are distributed according to a Maxwell-Boltzmann-Distribution at 0 K (using `ase.md.velocitydistribution.MaxwellBoltzmannDistribution`). Before deforming around 500 steps of the Verlet algorithm are run as to allow the system to reach a point at which the temperature is on average constant. Then the first of N_i strain steps is carried

out, after which the Verlet algorithm is run N_v times. This is repeated until the N_i-th step is reached. Trying different values for N_v and Δt leads to the conclusion, that for given strain rates making N_v larger is preferred. For values of Δt bigger than 0.1 fs. The temperature starts to 'explode'. The same outcome can be witnessed when the strain rate is chosen to be to high. E.g. a strain rate of $10^{14}\ s^{-1}$ with a value number of 60 for the Verlet-steps N_v leads to a strain of 0.6 after just one loop. This leads to a sudden temperature leap. For the following a lower strain rate is used.

4.3 Task 4.3: Energy Increase due to deformation - NVE-Ensemble

When deforming the total energy of the system is increasing. While the potential energy is staying the same the kinetic energy is increasing (coupled with a rise in temperature). For high strains, at a point the kinetic energy drops and the potential energy anti-symmetrically rises - leading to the total energy to stay stable at a higher level. This new level might be interpreted as the new equilibrium state. The increase in total energy could be coupled with the formation of new surfaces as a result of the alleged breaking of the specimen. The results for a simulation are plotted in fig. 10.

4.4 Task 4.4: Energy Increase due to deformation - NVT-Ensemble

Running the same simulation in a NVT-Ensemble yields a different result with respect to energies trajectories. The same setup as in section 4.3, was used but this time using the Langvin algorithm at a Temperature of 300 K and a friction term of $0.1 fs^{-1}$. For this the `ase.md.langevin` method was used. Resulting in fig. 11. The behaviourof the total energy is qualitatively the same, but contrary to what could be observed in the NVE simulation the kinetic energy approximately stays constant throughout the simulation. Whereas the potential is rising. This is due to the boundary conditions of the NVT-ensemble. The particles momenta are fixed on average. So the deformation of the specimen is not happening by a total change of the atoms velocities, but by individual changes for each particle. A result of this can be seen in fig. 12 - while in the NVE ensemble the temperature of the system is initially set to 0 K and as a response to strain being applied, the atoms are collectively accelerated, in the NVT ensemble the particles velocities are redistributed individually to keep the overall kinetic energy constant on average over time.

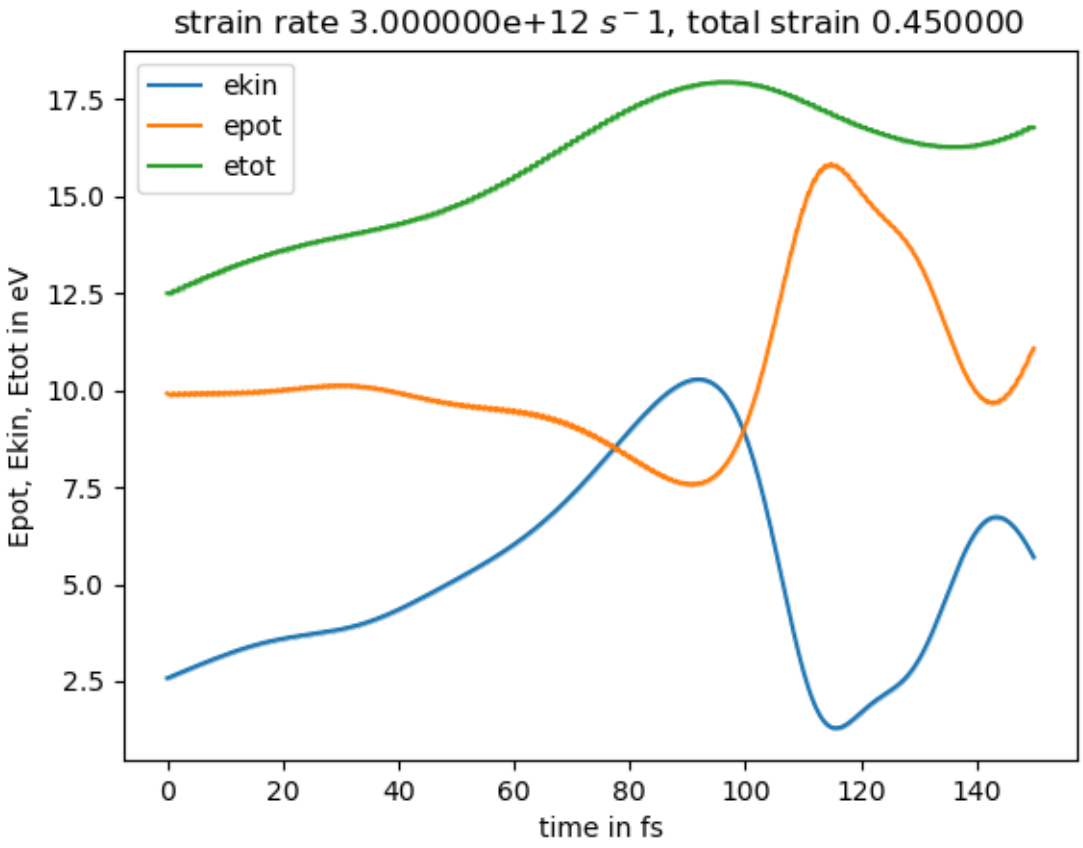

Figure 10: Potential, kinetic and total energy in eV plotted against time in fs at a strain-rate of $310^{12}s^{-1}$ simulated in a NVE-ensemble.

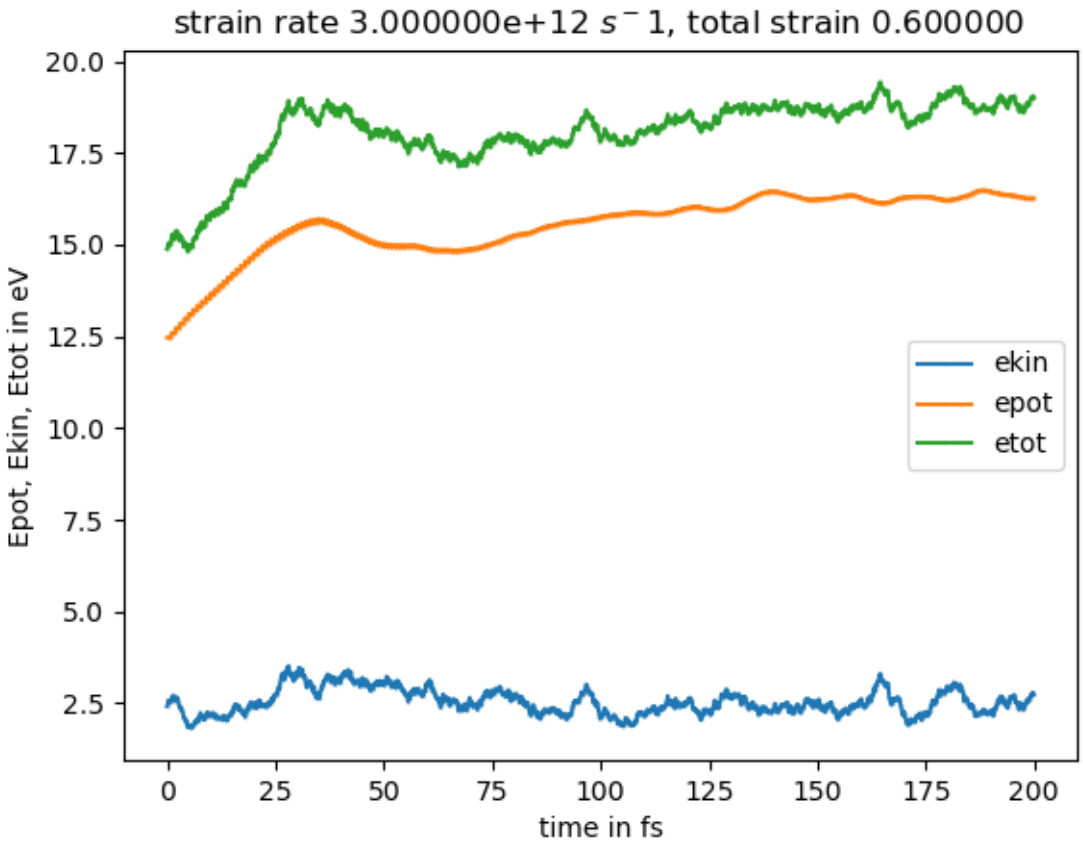

Figure 11: Potential, kinetic and total energy in eV plotted against time in fs at a strain-rate of $310^{12}s^{-1}$ simulated in a NVT-ensemble.

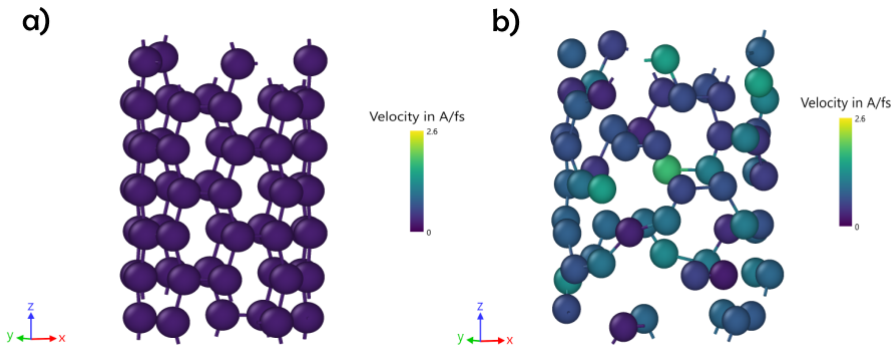

Figure 12: CNTs during deformation modeled in a a) NVE- b) NVT- ensemble. Color coding according to absolute value of the particles velocities. Visualized with OVITO [13].

4.5 Task 4.5: Bond breaking energy and how to theoretically obtain a stress-strain curve

To calculate the bond-breaking energy of the CNT the potntial energy after breaking and before deforming from sec. 4.4 is subtracted. This is resulting in a value of approximately 2.5 eV. Which is underestimating the bond energy of C-C bonds for which a literature of 3.60 eV can be found [2]. For calculating the stress-strain curve the atomic strains need to be calculated and plotted against the strain. The stress can be calculated with the following formula - based on the formula of virial stress [9]:

$$\boldsymbol{\sigma} = \frac{1}{V}\Big(-\sum_i m_i(v_i - \bar{v}) \otimes (v_i - \bar{v}) + \frac{1}{2}\sum_{i,j\neq i} r_{ij} \otimes f_{ij}\Big) \tag{12}$$

here V is the Volume in which we wan to calculate the stress, v_i is the velocity of the individual atom, $\bar{v}$ is the velocity on average, r_{ij} are the atoms' positions and f_{ij} the individual forces, that need to be derived from the potential.

5 Abbreviations

BCC	body centered cubic
DFT	density functional theory
EAM	embedded atom method
EMT	effective medium theory
FCC	face centered cubic
MWNT	multi-wall carbon nano-tubes
SC	simple cubic
SWNT	single-wall carbon nano-tubes

References

[1] Erik Bitzek et al. "Structural Relaxation Made Simple". In: *Physical Review Letters* 97.17 (Oct. 2006). Publisher: American Physical Society, p. 170201. DOI: 10.1103/PhysRevLett.97.170201. URL: https://link.aps.org/doi/10.1103/PhysRevLett.97.170201 (visited on 01/24/2024).

[2] *Bond Energies*. en. Oct. 2013. URL: https://chem.libretexts.org/Bookshelves/Physical_and_Theoretical_Chemistry_Textbook_Maps/Supplemental_Modules_(Physical_and_Theoretical_Chemistry)/Chemical_Bonding/Fundamentals_of_Chemical_Bonding/Bond_Energies (visited on 02/03/2024).

[3] David B. Graves and Pascal Brault. "Molecular dynamics for low temperature plasma–surface interaction studies". en. In: *Journal of Physics D: Applied Physics* 42.19 (Sept. 2009), p. 194011. ISSN: 0022-3727. DOI: 10.1088/0022-3727/42/19/194011. URL: https://dx.doi.org/10.1088/0022-3727/42/19/194011 (visited on 01/10/2024).

[4] William M. Haynes. *CRC Handbook of Chemistry and Physics*. en. Google-Books-ID: bNDMBQAAQBAJ. CRC Press, June 2014. ISBN: 978-1-4822-0868-9.

[5] K. W. Jacobsen, J. K. Norskov, and M. J. Puska. "Interatomic interactions in the effective-medium theory". In: *Physical Review B* 35.14 (May 1987). Publisher: American Physical Society, pp. 7423–7442. DOI: 10.1103/PhysRevB.35.7423. URL: https://link.aps.org/doi/10.1103/PhysRevB.35.7423 (visited on 01/08/2024).

[6] K. W. Jacobsen, P. Stoltze, and J. K. Nørskov. "A semi-empirical effective medium theory for metals and alloys". In: *Surface Science* 366.2 (Oct. 1996), pp. 394–402. ISSN: 0039-6028. DOI: 10.1016/0039-6028(96)00816-3. URL: https://www.sciencedirect.com/science/article/pii/0039602896008163 (visited on 12/20/2023).

[7] David W. Jacobson and Gregory B. Thompson. "Revisting Lennard Jones, Morse, and N-M potentials for metals". In: *Computational Materials Science* 205 (Apr. 2022), p. 111206. ISSN: 0927-0256. DOI: 10.1016/j.commatsci.2022.111206. URL: https://www.sciencedirect.com/science/article/pii/S0927025622000180 (visited on 01/08/2024).

[8] Y. Li et al. "Tensile properties of flexible carbon nanotube film/PVA composite at various strain rates". English. In: *Polymer Composites* 44.9 (2023), pp. 6164–6177. ISSN: 0272-8397. DOI: 10.1002/pc.27554.

[9] Bin Liu and Xingming Qiu. *How to Compute the Atomic Stress Objectively?: Ingenta Connect*. URL: https://www.ingentaconnect.com/contentone/asp/jctn/2009/00000006/00000005/art00019 (visited on 02/03/2024).

[10] Marc Monthioux et al. "Introduction to Carbon Nanotubes". en. In: *Springer Handbook of Nanotechnology*. Ed. by Bharat Bhushan. Springer Handbooks. Berlin, Heidelberg: Springer, 2007, pp. 43–112. ISBN: 978-3-540-29857-1. DOI: 10.1007/978-3-540-29857-1_3. URL: https://doi.org/10.1007/978-3-540-29857-1_3 (visited on 01/24/2024).

[11] J. J. More, B. S. Garbow, and K. E. Hillstrom. *User guide for MINPACK-1. [In FORTRAN]*. English. Tech. rep. ANL-80-74. Argonne National Lab. (ANL), Argonne, IL (United States), Aug. 1980. DOI: 10.2172/6997568. URL: https://www.osti.gov/biblio/6997568 (visited on 01/15/2024).

[12] W. C. Overton and John Gaffney. "Temperature Variation of the Elastic Constants of Cubic Elements. I. Copper". In: *Physical Review* 98.4 (May 1955). Publisher: American Physical Society, pp. 969–977. DOI: 10.1103/PhysRev.98.969. URL: https://link.aps.org/doi/10.1103/PhysRev.98.969 (visited on 01/24/2024).

[13] Alexander Stukowski. "Visualization and analysis of atomistic simulation data with OVITO–the Open Visualization Tool". en. In: *Modelling and Simulation in Materials Science and Engineering* 18.1 (Dec. 2009), p. 015012. ISSN: 0965-0393. DOI: 10.1088/0965-0393/18/1/015012. URL: https://dx.doi.org/10.1088/0965-0393/18/1/015012 (visited on 02/03/2024).

[14] *The Lennard-Jones potential — ASAP3*. URL: https://asap3.readthedocs.io/en/latest/manual/potentials/Lennard-Jones.html#lennard-jones (visited on 01/08/2024).

[15] Kazufumi Yoneyama et al. "Mechanical properties of carbon nanotube under uniaxial tensile strain". en. In: *Japanese Journal of Applied Physics* 59.SI (Apr. 2020). Publisher: IOP Publishing, SIID02. ISSN: 1347-4065. DOI: 10.35848/1347-4065/ab7f5a. URL: https://dx.doi.org/10.35848/1347-4065/ab7f5a (visited on 01/26/2024).